Optimization of Magnetic Field Based on Electron Orbit Measurement in TOKASTAR-2 Helical Plasmas*)

Keitaro KADO, Takaaki FUJITA, Atsushi OKAMOTO, Hideki ARIMOTO, Keishi TSUNODA and Shunsuke MORIZAWA

Graduate School of Engineering, Nagoya University, Furo-sho, Chikusa-ku, Nagoya 464-8603, Japan

(Received 10 January 2022 / Accepted 19 April 2022)

By using newly installed local helical coils (ULT coils), it is expected that helical magnetic field will be reinforced and then the rotational transform and the cross-sectional area of the last closed flux surface (LCFS) will get larger in TOKASTAR-2. Electron beam mapping and plasma measurement with an electrostatic probe were made to confirm improvement in the helical field. As the result, large closed flux surfaces were measured by using the ULT coils. In plasma measurement, it was observed that the plasma pressure changed according to the movement of the calculated LCFS, though change in the plasma pressure at the position of the calculated LCFS was not clear. Furthermore, it was confirmed that helical magnetic field confined plasma from plasma decay after turning off the plasma heating power.

Keywords: TOKASTAR-2, stellarator, closed flux surface, electron orbit trace, triple probe measurement

DOI: 10.1585/pfr.17.2402071

1. Introduction

TOKASTAR-2 is a small tokamak-stellarator hybrid device equipped with local helical coils (Fig. 1). The research objectives include study on tokamak-stellarator hybrid configurations and study on effects of helical field on tokamak plasma. Stabilization effects of the helical field was observed on the plasma horizontal position [1–3]. Those on the plasma vertical position was, however, not clear [4]. According to field line calculation, it was possible to generate closed flux surfaces (LCFSs) in vacuum with local helical coils. However, the helical field was weak and therefore the rotational transform and cross-sectional area of the LCFS were small.

The problem was that effective radial field made by upper/lower local helical coils, AHF coils, was weak because they are located 230 mm away from the equatorial plane; the distance is six times as large as the plasma minor radius, 40 mm. To reinforce effective radial magnetic field, new local helical coils (ULT coils) have been designed and fabricated [4]. Four ULT coils, two on upper side and two on lower side were installed inside of the toroidal field (TF) coils, as shown in Fig. 2. By using ULT coils, it is expected that rotational transform gets larger from around 0.01 to 0.02, and large closed flux surface are obtained. An examle is shown in Fig. 3. The horizontal width is 80 mm. This is significantly larger than that of the LCFS obtained previously; for instance it was 40 mm in the LCFS shown in Fig. 7 of Ref. [5]. In tokamak experiment, effects on the vertical instability was observed with using ULT coils

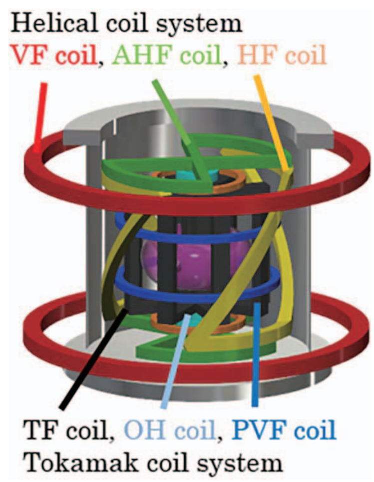

Fig. 1 Coil systems in TOKASTAR-2.

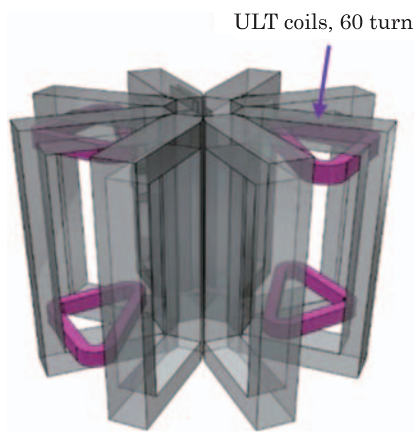

Fig. 2 ULT coils (pink) installed inside TF coils (grey).

Corresponding author's e-mail: fujita@energy.nagoya-u.ac.jp

*) This article is based on the presentation at the 30th International Toki Conference on Plasma and Fusion Research (ITC30).

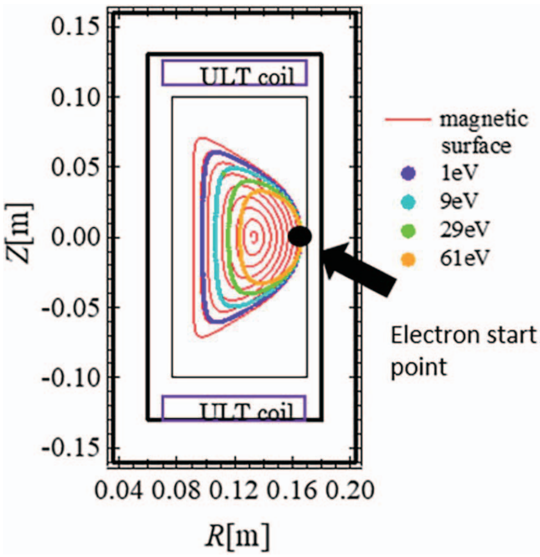

Fig. 3 Example of flux surfaces and electron orbits at toroidal angle $\phi = 0$ in a magnetic field generated with ULT coils. The TF coil current is 7.5 kAturn, the HF coil current is −2.5 kAturn, all ULT coil currents are −2.5 kAturn, and the VF coil current is 0.25 kAturn. The toroidal magnetic field strength at $R = 0.12$ m, $Z = 0$ m is $B_t = 0.1$ T and the poloidal magnetic field strength at the electron start point is $B_p = 0.001$ T.

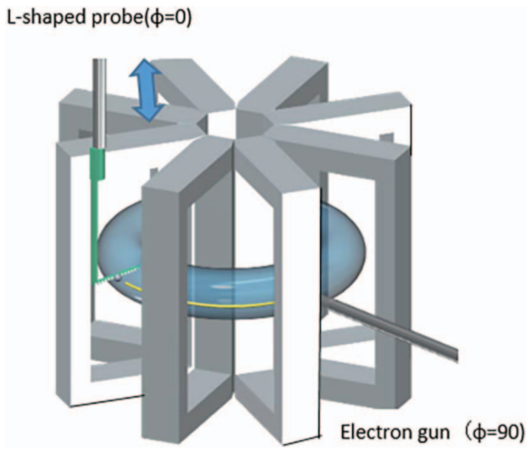

Fig. 4 Layout of the electron gun and the L-shaped probe.

[6]. The purpose of this work is to confirm improvement of vacuum helical field with ULT coils by two methods; (i) electron beam mapping in vacuum and (ii) plasma measurement with an electrostatic probe.

2. Experiment Tools of Electron Beam Mapping

Electron beam mapping is one of methods to obtain poloidal cross-sections of flux surfaces. Since electrons travels basically along the field line, flux surfaces can be obtained by catching electrons. In TOKASTAR-2, two tools are used: an electron gun and an L-shaped probe. The former generates an electron beam while the latter detects electrons. Although a fluorescent mesh is frequently used to detect electrons in electron beam mapping [7, 8], we have found that electron energy larger than 80 eV is required to observe the fluorescence in previous study [9]. We considered that deviation of orbit of 80 eV electrons is unacceptably large in TOKASTAR-2 and then decided not to use the fluorescent mesh but to use the probe to detect electrons [9]. It should be noted, however, that the distance between the fluorescent mesh and the electron gun was only 10 cm in a test chamber without magnetic field in the experiment in Ref. [9]. In this layout, the light from the hot filament directly illuminated the mesh and hindered detection of weak fluorescent light. The conditions would be improved in TOKASTAR-2, where direct illumination can be avoided.

The electron gun is inserted through a horizontal gauge port, while the L-shape probe is inserted through a vertical gauge port, as shown in Fig. 4. They are located 90 degrees apart in the toroidal direction. The angle where the L-shape probe is located is defined as $\phi = 0°$ and the angle of the electron gun is $\phi = 90°$. In previous study [9], an old electron gun was directly attached to one of four large horizontal port flanges with outer diameter of 265 mm. This port is usually used for injection of microwave to generate and heat plasma. It was thus needed to vent the vacuum vessel and remove and attach large port flanges both for installing and for removing the electron gun, and therefore chance for the electron beam mapping was quite limited. The present electron gun was developed to allow permanent installation to the device. The vertical position of the electron gun can be changed among $Z = 45$ mm, 0 mm and −45 mm by selecting a gauge port. In this work, the gun was located at $Z = -45$ mm. The radial position of the gun can be changed between shots.

The electrical circuit of the electron gun is shown in Fig. 5. A filament is located inside a holder with a square pole shape. The height and the width of cross-section of the holder are 6.5 mm and 13.5 mm, respectively. Electrons are emitted from the tungsten filament by heating it with current. A tungsten wire with a diameter of 0.15 mm is wound into a filament coil with an inner diameter of 0.5 mm and a length of 7 mm. The emitted electron current is several mA with the filament current of 2.1 A. The electrons are extracted through a hole of the holder by applying a voltage of 30 V between the filament and the holder, the latter of which is connected electrically to the vacuum vessel or the limiter. The acceleration voltage can be adjusted between 0 V and 100 V. The voltage of 30 V is the minimum value required for extracting an enough amount of electronic beam. Then electron Larmor radius is 0.18 mm at $B_t = 0.1$ T. The beam current of several μA is measured with a probe located at the same R and Z as the hole of the holder and apart 45 mm toroidally from it. But it finally decays to 0.1 μA at minimum when it is detected with the L-shaped probe. This value is the same order as back-

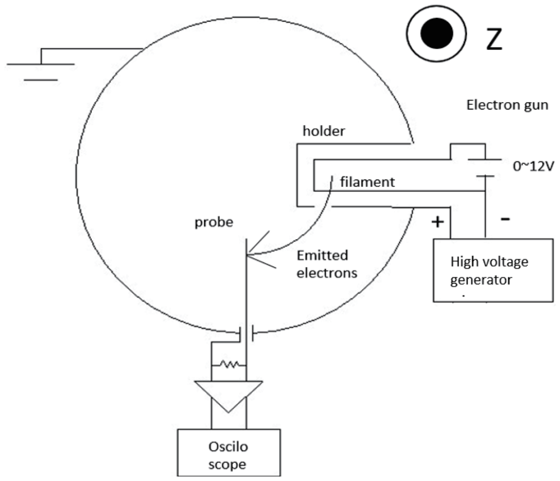

Fig. 5 Electrical circuits of the electron gun and the L-shaped probe.

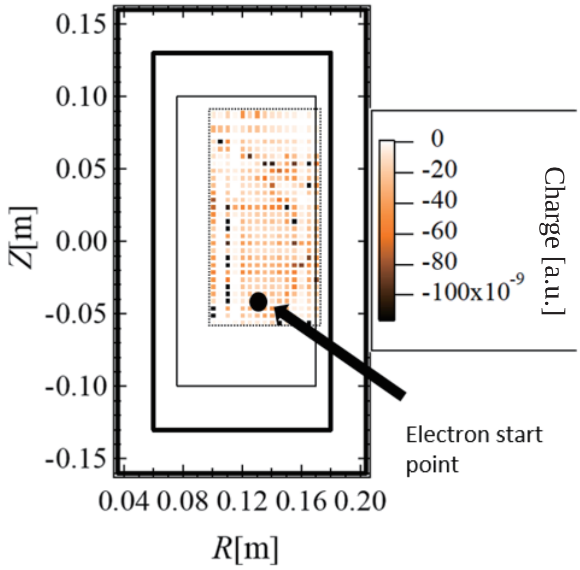

Fig. 6 Spatial distribution of raw signal at I_{TF} = 4.0 kAturn and B_{t} = 0.053 T.

ground. The cause of this decay seems that some electrons will collide and spread while they travel around the torus many times. So attention should be paid to residual gas pressure, which is 6×10^{-4} Pa in the present experiment. The decay is larger for orbits with longer length that is expected when the field pitch angle is small.

The L-shaped probe has 15 stainless electrodes 3 mm square. The electrodes are connected to the vessel through a resistor of 12 kΩ as shown in Fig. 5. The current of electron caught by each electrode is evaluated from the voltage of the resistor. The value of the resistance was decided considering time response of the measurement and also that the voltage generated by electrons would be sufficiently lower than the acceleration voltage. The electrodes are aligned radially with a distance of 5 mm between centers. By scanning the L-shaped probe vertically as shown in Fig. 4 between shots, passing points of electrons are measured in the poloidal plane. In the experiment shown in this work, the vertical position was moved every 5 mm, and then the spatial resolution was 5 mm both in radial and vertical directions. The sampling rate of the voltage was 1 μs.

3. Measurement and Analysis of Electron Beam Mapping

An example of actually measured raw signals in *RZ* plane at $\phi = 0°$ is shown in Fig. 6. The outer frame with thick solid lines denotes the TF coil, and the inner rectangle with thin solid line denotes the limiter equipped at $\phi = 202.5°$. It limits plasma in the area of $0.0754\,\mathrm{m} \leq R \leq 0.171\,\mathrm{m}$ and $-0.10\,\mathrm{m} \leq Z \leq 0.10\,\mathrm{m}$. The smallest dotted rectangle shows the area measured by the L-shaped probe, $0.099\,\mathrm{m} < R < 0.169\,\mathrm{m}$, $-0.06\,\mathrm{m} < Z < 0.09\,\mathrm{m}$. In the measurement, the TF coil was in pulse operation with the peak current of ~150 A per conductor or ~7.5 kAturn per coil; each TF coil has 50 turns. The other coils were in steady operation. The HF coil current was −2.5 kAturn, the upper ULT coil current was −2.5 kAturn, the lower ULT coil current was −1.5 kAturn, and the VF coil current was 0.4 kAturn. Electrons were injected from the gun continuously during the measurement period. The same conditions were used for coil currents in all of the data shown in following sections, both for electron mapping and for plasma measurement. The electron current measured by the probe was integrated for 0.1 ms to reduce the fluctuations and then the results are shown in charge.

In Fig. 6, electron signals are detected in most of the measured points and then the shape of the orbit surface is not clearly recognized. Raw signals contain electrons diffused from the orbit surface since electrons were continuously injected. In order to eliminate the effect of diffused electrons, signals lower than a threshold corresponding to the background level were truncated. Furthermore, log scale plot was adopted because of a wide range of signals.

Magnetic field lines and electron orbits were calculated to be compared with the experimental results. The calculation procedure is as follows: (i) magnetic field vector is calculated at the initial position by Biot-Savart law, (ii) the guiding center velocity including the drift velocity is calculated in case of electron orbit, (iii) the position is advanced in a small distance, (iv) the calculation is repeated until the surface of the TF coils or the surface of the limiter is encountered. The toroidal position of the limiter is taken into account for judging the contact with the limiter, while the axisymmetric boundary is assumed for the TF coil surface.

4. Results of Electron Beam Mapping

Figure 7 shows results of electron beam mapping. The

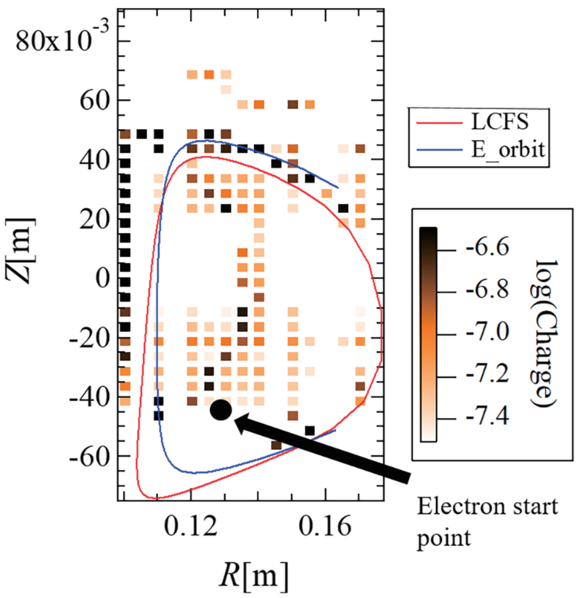

Fig. 7 Measured electron signals and calculated LCFS and the orbit of electrons with 30 eV at I_{TF} = 5.0 kAturn and B_t = 0.067 T. In calculation of the electron orbit, the electron was started not from the hole of the electron gun shown in the figure but from a point on the calculated last closed flux surface.

detected charge at each point was denoted by color of the small square, as shown in color bars. The LCFS and the electron orbit were evaluated at the same toroidal angle of the L-shape probe in calculation, which are shown by red thin lines and dark blue symbol, respectively. In the signals of electron beam mapping, it is considered that continuous black points result from electrons that travelled along the field line while the orange points result from diffused electrons. In electron beam mapping, a closed and large flux surface, similar to that predicted by field line calculation and electron orbit calculation, is recognized, but the internal structure was different from calculation where nested structure is expected as shown in Fig. 3. This suggests existence of error fields.

5. Electrostatic Probe Measurement

By measuring the radial distributions of plasma, we would be able to evaluate effects on plasma confinement of the flux surface structure and compare it with electron beam mapping. Plasma density and temperature were measured with a triple probe. The working gas was nitrogen. Electron cyclotron (EC) heating with 2.45 GHz microwave was used to generate plasma. The plasma with the toroidal field only, namely without helical field, was also measured for comparison. The probe used is the same as used in Ref. [5]. The probe was inserted on the equator plane (Z = 0 mm) and its radial position was changed between shots to obtain the radial profiles. Three tips of the probe are in a cylindrical shape with a diameter of 0.6 mm and a

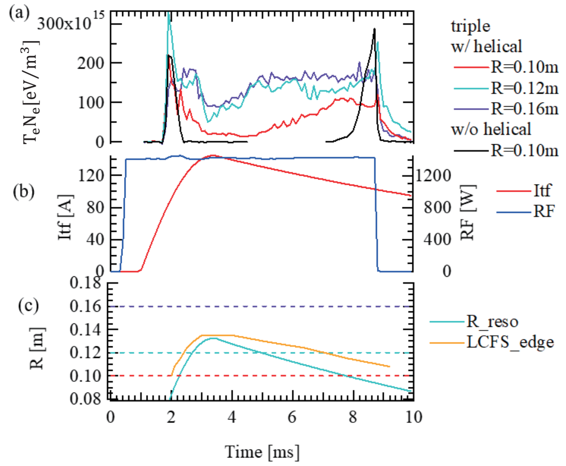

Fig. 8 (a) Time evolution of the plasma pressure T_eN_e measured with the triple probe at R = 0.10, 0.12, 0.16 m with helical field and R = 0.10 m without helical field. (b) Time evolution of the TF coil current (in red) and the microwave power (in blue). (c) Time evolution of the major radius of the EC resonance layer (in light blue) and the inner LCFS (in yellow).

length of 2.0 mm. The applied voltage for measurement of the ion saturation current was 36 V. The measured electron density was averaged for 0.1 ms to reduce the fluctuations. The EC resonance radius moves according to the TF coil current. The LCFS also moves according to the TF coil current as shown in Ref. [5].

The results are shown in Fig. 8. The electron pressure was evaluated by the product of the electron density and the electron temperature measured by the triple probe. The electron pressure at R = 0.10 m and R = 0.12 m decreased when the measured positions were located far from the LCFS. However change in the plasma pressure at the position of the calculated LCFS was not clear. Although the EC resonance position also moved as shown in Fig. 8 (c), the waveform was different when the helical field was not applied, where nearly zero pressure was observed inside the resonance position. This suggests the difference of confinement due to existence of helical field., even outside the LCFS.

In Fig. 8 (a), it is recognized that the plasma pressure decays slower in the case with the helical field than without the helical field. From decay of plasma pressure, plasma confinement effect of helical plasma can be evaluated. The time evolution of the plasma pressure around turning off the microwave at t = 8.8 ms is shown in Fig. 9 with expanded view, while the radial profiles of the plasma pressure are shown in Fig. 10. Plasma disappeared quickly without helical field while it remained for a while with helical field. The pressure drop in the case without helical field before turning off the RF power is not real but caused by averaging the data for 0.1 ms. The pressure peak around R = 0.13 m observed at t = 8.05 ms and 8.85 ms seems to correspond to the location of the magnetic axis.

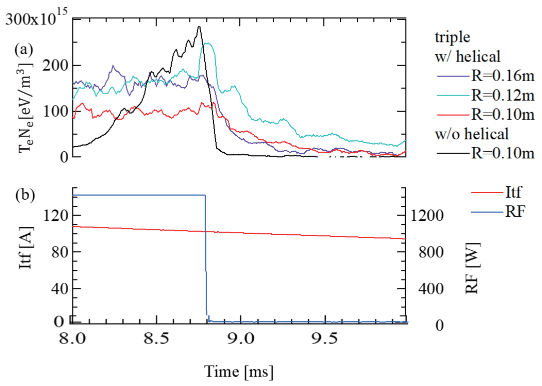

Fig. 9 Expanded view of Fig. 8 (a) and (b).

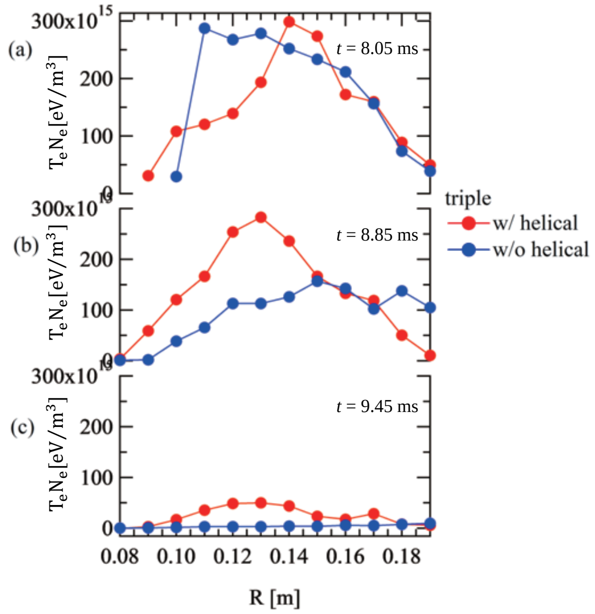

Fig. 10 Radial profiles of plasma pressure (a) before and (b) (c) after turning off the microwave power. The red and blue lines denote the case with the helical field and that without the helical field, respectively.

6. Summary

Electron beam mapping was made with an electron gun and an L-shaped probe in helical field generated with newly installed local helical coils (ULT coils) in TOKASTAR-2. Large flux surfaces were measured, as predicted by field line calculation. But the structure inside the last closed flux surface (LCFS) was different from calculation, which suggests existence of error fields.

The radial distribution of the electron pressure in helical plasma was measured with a triple probe. It was observed that the electron pressure changed according to the movement of the calculated LCFS and the EC resonance layer. Furthermore, plasma confinement with helical field was confirmed from the electron pressure decay after turning off the microwave power.

Acknowledgments

This work was performed with the support and under the auspices of the NIFS Collaboration Research program (NIFS20KLEP038, NIFS20KBAH031) including the NIFS Joint Use Program of Measurement Instruments.

[1] T. Ueda *et al.*, Plasma Fusion Res. **10**, 3402065 (2015).
[2] T. Sakito *et al.*, Plasma Fusion Res. **11**, 2402074 (2016).
[3] K. Yasuda *et al.*, Plasma Fusion Res. **13**, 3402072 (2018).
[4] K. Yasuda *et al.*, Plasma Fusion Res. **15**, 1402083 (2020).
[5] H. Itou *et al.*, Plasma Fusion Res. **13**, 1402039 (2018).
[6] K. Yasuda *et al.*, Phys. Plasmas **28**, 082108 (2021).
[7] R.J. Colchin *et al.*, Rev. Sci. Instrum. **60**, 2680 (1989).
[8] H. Yamada *et al.*, Rev. Sci. Instrum. **61**, 686 (1990).
[9] Y. Shimooka *et al.*, Plasma Fusion Res. **11**, 2402110 (2016).